ELSEVIER

Earth and Planetary Science Letters 210 (2003) 545–560

EPSL

www.elsevier.com/locate/epsl

Flexural subsidence by 29 Ma on the NE edge of Tibet from the magnetostratigraphy of Linxia Basin, China

Xiaomin Fang [a,b], Carmala Garzione [c,*], Rob Van der Voo [d], Jijun Li [a], Majie Fan [a]

[a] *MOE National Laboratory of Western China's Environmental Systems and College of Resources and Environment, Lanzhou University, Lanzhou, Gansu 730000, PR China*

[b] *State Key Laboratory of Loess and Quaternary Geology, Institute of Earth Environment, CAS, Xi'an, Shanxi 710054, China*

[c] *Department of Earth and Environmental Sciences, University of Rochester, Rochester, NY 14627, USA*

[d] *Department of Geological Sciences, University of Michigan, Ann Arbor, MI 48109, USA*

Received 24 October 2002; received in revised form 24 February 2003; accepted 28 February 2003

Abstract

This study provides a detailed magnetostratigraphic record of subsidence in the Linxia Basin, documenting a 27 Myr long sedimentary record from the northeastern edge of the Tibetan Plateau. Deposition in the Linxia Basin began at ~29 Ma and continued nearly uninterruptedly until ~1.7 Ma. Increasing rates of subsidence between 29 and 6 Ma in the Linxia Basin suggest deposition in the foredeep portion of a flexural basin and constrain the timing of shortening in the northeastern margin of the plateau to Late Oligocene–Late Miocene time. By Late Miocene–Early Pliocene time, a decrease in subsidence rates in the Linxia Basin associated with thrust faulting and a ~10° clockwise rotation in the basin indicates that the deformation front of the Tibetan plateau had propagated into the currently deforming region northeast of the plateau.

Keywords: Asia; magnetostratigraphy; flexural basin; fold and thrust belt; Tibetan Plateau

1. Introduction

The timing and mechanisms of growth of the Tibetan Plateau are still poorly understood because of a lack of widespread and precise constraints on the timing of deformation in the plateau. Along the northeastern edge of the Tibetan Plateau, fold-thrust belts, such as the Nan Shan, Qilian Shan, and Liupan Shan, are presently undergoing shortening as they are incorporated into the plateau [1–5] (Fig. 1A). Today, strike-slip deformation dominates the northern part of the Tibetan Plateau [1]. It has been suggested that left slip at the eastern termination of the Altyn Tagh fault is absorbed by northeast-directed shortening, accommodating growth of the northeastern part of the plateau [2,3,6], whereas transpressional deformation is occurring in the Liupan

* Corresponding author. Tel.: +1-716-273-4572; Fax: +1-716-244-5689.
E-mail address: garzione@earth.rochester.edu (C. Garzione).

0012-821X/03/$ – see front matter
doi:10.1016/S0012-821X(03)00142-0

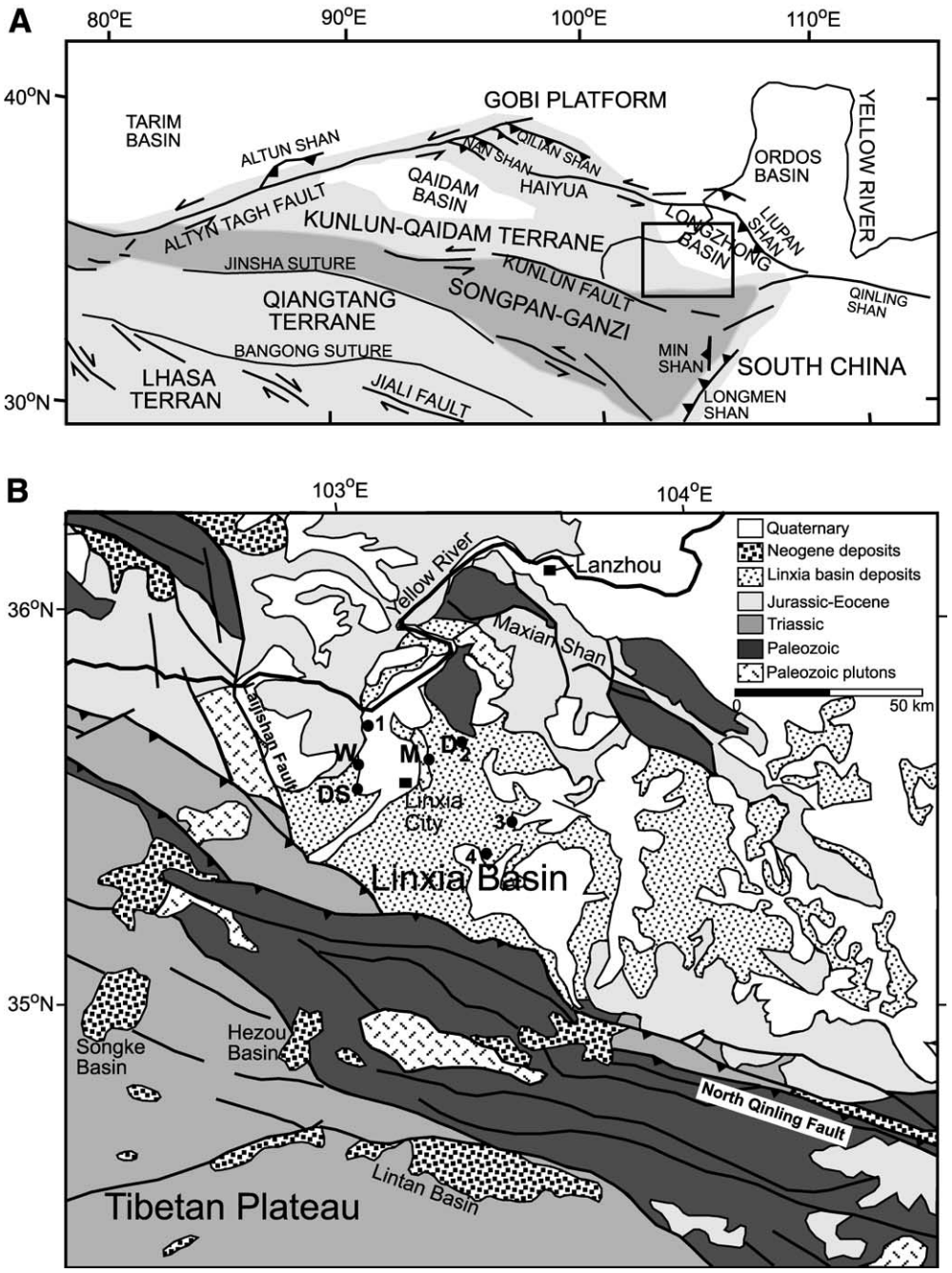

Fig. 1. (A) Location of the study area (rectangle) relative to major tectonic elements of the Tibetan Plateau (simplified from [4]). The gray region shows the extent of the Tibetan Plateau. The darker gray region shows the extent of the Songpan–Ganzi accretionary wedge. (B) Simplified geologic map of the Linxia Basin on the northeastern margin of the Tibetan Plateau [19], showing localities of studied sections and fossil mammals in the Linxia Basin. Thick lines are faults. Teeth are shown in the hanging wall of thrust faults. Black dots show locations of measured sections: Wangjiashan (W), Maogou (M), Dongxiang (D), and Dongshanding (DS); and faunal assemblages: Longguan fauna (1), Longdan fauna (2), Sigou fauna (3), and Shanzhuang fauna (4).

Shan at a southward bend in the east–southeast-striking Haiyuan fault [3,4,6] (Fig. 1A). GPS measurements across northeastern Tibet show that this region is moving NE–NNE at velocities of 19–15 mm/yr relative to the fixed South China Block [7]. However, localities in the foreland, north of the Altyn Tagh fault and Qilian Shan, display much lower and more northerly velocities of 4–10 mm/yr relative to South China [7], indicating that the northeastern part of the plateau is moving eastward relative to the northern foreland.

Widespread deformation and associated sedimentary basin deposition across the Tibetan Plateau provide a record of upper crustal shortening in the plateau. Based on the age of magmatism, deformation, and the seismic structure of the lithosphere at significant tectonic boundaries in the plateau, it has been suggested that deformation took place from south to north, causing stepwise uplift of the Tibetan Plateau [8]. Age constraints from sedimentary fill in a flexural basin in the eastern Qiangtang Block document Cretaceous–Paleogene deformation associated with thrust faulting, whereas strike-slip faults in this region postdate basin development [9]. Volcanic rocks unconformably overlying and intruding these deposits constrain the youngest sedimentation to Middle–Late Eocene age [9]. The Eocene age for shortening in this region is corroborated by a belt of ~50–40 Ma magmatism in the Tanggula mountains, which has been interpreted as resulting from the southward subduction of Asian lithosphere along the Jinsha suture along the Eocene edge of the high Tibetan Plateau as it existed at that time [8,10].

Along the northern margin of the plateau, initial deformation in Eocene–Oligocene time has been inferred from apatite fission track analyses from rocks along the Altyn Tagh and Kunlun faults surrounding the Qaidam Basin [11,12]. These data are supported by seismic data from northern Qaidam, which show growth strata that indicate deformation began by at least Oligocene time [13]. Magnetostratigraphic ages from the southern Tarim Basin corroborate these data, indicating an initial age of crustal thickening of ~49 Ma on the margins of the Qaidam Basin and ~33 Ma for the Nan Shan fold-thrust belt, northeast of Qaidam [14]. Yin et al. [14] interpret these thrust systems as forming in relation to the Altyn Tagh fault, which suggests initiation of strike-slip deformation by 49 Ma. However, Tertiary piercing points from the central and eastern portion of the Altyn Tagh fault have been interpreted to suggest a younger age of initial strike-slip motion of Late Oligocene–Early Miocene [15]. Stratigraphic patterns and paleocurrent indicators also suggest that Tarim and Qaidam basins were separated by the Altyn Tagh fault by Miocene time [16]. This strike-slip deformation led to an increase in exhumation in the Qilian Shan, as well as the Kunlun Shan and Altun Shan, in Miocene–Pliocene time, recorded by apatite fission track ages [11,17]. Increasing rates of exhumation in the Qilian Shan in Pliocene–Quaternary time have been interpreted based on an increase in sediment accumulation rates at ~6 Ma and the deposition of a thick gravel succession of upper Pliocene–Pleistocene age [5,18]. The growing number of studies of the northern margin of the Tibetan Plateau continues to support the notion that deformation associated with the Altyn Tagh fault propagated towards the northeast through time. Linxia Basin deposits provide a unique opportunity to place spatial and temporal constraints on the deformation history of the northeastern margin of the Tibetan Plateau. In this study, we report on the magnetostratigraphy of the Linxia Basin, thereby documenting both the timing and mechanisms of subsidence in this region. This is the longest magnetostratigraphic record, in terms of time, documented from the terrestrial Cenozoic.

2. Geologic background

The Linxia Basin is a sub-basin of the Longzhong Basin, located just northeast of the topographic front on the northeastern edge of the Tibetan Plateau and south of the Haiyuan fault, a large-scale, left-lateral, strike-slip fault [4,6], and the Liupan Shan to the northeast (Fig. 1A). The lateral extent of Linxia Basin is marked by structural boundaries on the northern, western, and

southern edges of the basin, but is poorly defined towards the east. To the west and south, the major basin-bounding faults within the Tibetan Plateau are the Laijishan fault and North Qinling fault, respectively (Fig. 1B). Linxia Basin sedimentary rocks onlap Cretaceous sedimentary rocks in the Maxian Shan to the north (Fig. 1B). Throughout the central part of the Linxia Basin, the oldest deposits were laid down on granite of inferred Paleozoic age [19]. Southwest of the Linxia Basin, the Tibetan Plateau consists of Devonian–Permian terrestrial and marine deposits of the Kunlun–Qaidam terrane and Triassic submarine fan deposits of the Songpan–Ganzi accretionary wedge, which were shed by the east–southeast striking Qinling mountain belt to the east of the plateau (Fig. 1A) [20–22].

3. Linxia Basin stratigraphy

Sedimentary rocks of the Linxia Basin are dominated by mudstone and sandstone of fluvial and lacustrine origin. The stratigraphy has been subdivided into eight formations based on lithofacies, contacts and paleontology (Fig. 2), and can be traced across the basin. Three stratigraphic sections were measured along a profile perpendicular to the northeastern margin of the Tibetan Plateau (Fig. 2). These sections provide a proximal to distal profile across the basin from the Tibetan Plateau margin towards the Maxian Shan. Both the most proximal Wangjiashan (WJS) and central Maogou sections contain lithologies that can be correlated to one another. The more distal Dongxiang section, which is dominantly mudstone, cannot be easily correlated based on lithology and therefore only provides information on the variation in stratigraphic thickness and grain size across the basin.

The lower six formations are dominantly red mudstone and yellowish-gray sandstone. In the WJS section, these deposits have been folded during thrusting to form an anticline with an approx-

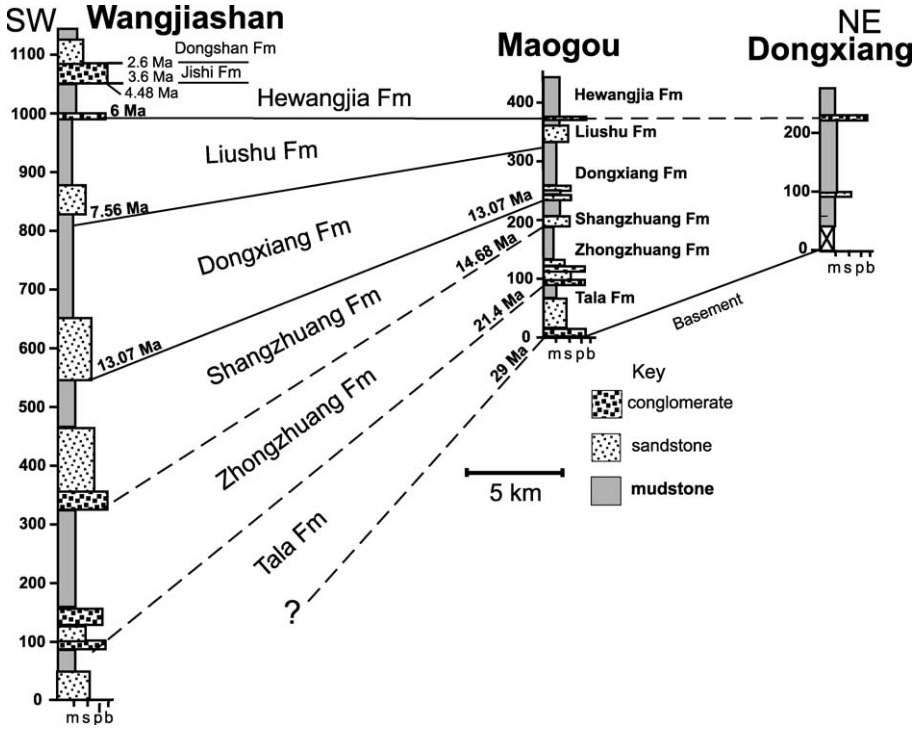

Fig. 2. Stratigraphic correlation between the three measured sections in the Linxia Basin. Solid lines are based on magnetostratigraphic correlation. Dashed lines are correlations based on lithofacies and mammalian fauna. Section locations are shown in Fig. 1B.

imately N–NE-trending fold axis. These formations include the Tala through Hewangjia formations and are characterized by six cycles (formations) of fining-upward gray to yellow, cross-bedded or massive pebbly sandstone and pebble–cobble conglomerate to yellowish-brown, laminated mudstone or red massive to laminated mudstone (Fig. 2). Lithostratigraphic correlations between the WJS and Maogou sections are drawn based on these grain-size trends and agree with magnetostratigraphic correlations between the upper 600 m of the WJS section and the upper 200 m of the Maogou section. The Tala and basal Zhongzhuang formations are represented by fluvial channel and floodplain deposits. By ~19 Ma, widespread lacustrine deposition was established throughout the basin. During deposition of the Shangzhuang through basal Liushu formations, two fining-upward cycles represent marginal lacustrine facies (central part of the basin) and fluvial facies (proximal part of the basin) at the base of the formations grading up into lacustrine fa-

Table 1
Fossil mammals found in and near the studied sections in the Linxia Basin

Mammal layer[a]	Mammals	Chinese mammal stage and age	Locality[c]	Ref.
1	*Equus sanmeniensis*, *Lynx* sp. (*L. shansius*?) and *Gazella* sp.; Longdan fauna: *Vulpes* sp., *Canis* cf. *C. chihliensis*, *Pannonictis* cf. *P. pachygnathus*, *Pachycrocuta licenti*, *Lynx* sp., *Nestoritherium* sp., *Coelodonta* cf. *C. nihowanensis*, *Meles* sp., *Megantereon* cf. *M. nihowanense*, *Homotherium* cf. *H. nestianum*, *Sivapanthera* sp., *Equus* sp. nov., *Sciuridae* gen. et sp. nov., *Macaca* sp., *Procynocephalus* sp., *Sinocuon* sp., *Felis* cf. *F. palaeosinensis*, *Leptobos* sp., etc.	Nihewan, ~2 Ma (Villafranchian)[b]	2, W	[25,29]
2	*Hipparion* sp.	Jinglean, 3.4–5.2 Ma (Ruscinian)[b]	W	[25]
3	Giraffidae gen. et sp. indet.; Longguan fauna: *Machairodus* (*Epimachairodus*?) cf. *ultimus*, *Indarctos* sp., *Ictitherium gaudryi*, *Adcrocuta* cf. *eximia variabilis*, *Hipparion* (*Hipparion*) *platyodus*, *H.* (*H.*) *fossatum*, *Hipparion* (*Cremohipparion*) cf. *licenti*, *Acerorhinus linxiaensis* sp. nov., *A. palaeosinensis*, *Chilotherium* (*Chilotherium*) *anderssoni*, *C. gracile*, *Gazella gaudryi*, *Antilope* sp., *Cervavitus novorossiae*, *Propotamochoerus* sp.	Baodean, 5.2–9 Ma (Turolian)[b]	4, 1, M	[30,31]
4	*Hipparion* sp., *Chilotherium* sp., *Honanotherium* sp., *Cervavitus* sp., *Protalactaga* cf. *tunggurensis*, Spalacinae gen. indet., Castoridae gen indet., *Ochotona lagrelii minor*, *Ictitherium hipparionum hyaenoides*, *Adcrocuta* cf. *eximia variabilis*		1	[32]
5	Sigou fauna: *Dinocrocuta gigantea*, *Adcrocuta eximia varibilis*, *Ictitherium wongii*, *H.* cf. *chiai*, *Hipparion platyodus*, *H.* cf. *chiai*, *H.* cf. *fossafum*, *H.* cf. *hippidiodus*, *H.* cf. *tchicorcum*, *Chilotherium* sp., *Ninxiatherium* cf. *longirhinus*, *Palaeotragus* cf. *microdon*, *Cervavitus novorossiae*, *Gazella gaudryi*, *G.* cf. *dorcadoides*, *Tetralophodon exoletus*, *Serridentinus* sp., *T.* cf. *xaolongtanensis* (?), *Gomphotherium* cf. *hopwoodi*, *Hipparion* cf. *hippidiodus sefve*, *Gazella* sp.	Bahean, 9–12.5 Ma (Vallesian)[b]	1	[25,30]
6	Shanzhuang fauna: *Giraffokeryx shanzhuangensis* sp. nov., *Hipparion*, *Chilotherium*, *Platybelodon*, *Honanotherium*, Mustelidae, *Struthis*	Tongguerean, 12.5–15.4 Ma (Astaracian)[b]	3	[30]
7	*Gomphotherium* sp., *Dzungariotherium orgosense*, Rhinocerotidae gen. indet., *Paraentelodon macrognathus* sp. nov.	Early Xiejian, ~21 Ma (E. Orleanian)[b]	M, 2	[28,30]

[a] These numbers denote stratigraphic levels and are shown in Fig. 3.
[b] Equivalent European land mammal stage.
[c] Locations are shown in Fig. 1.

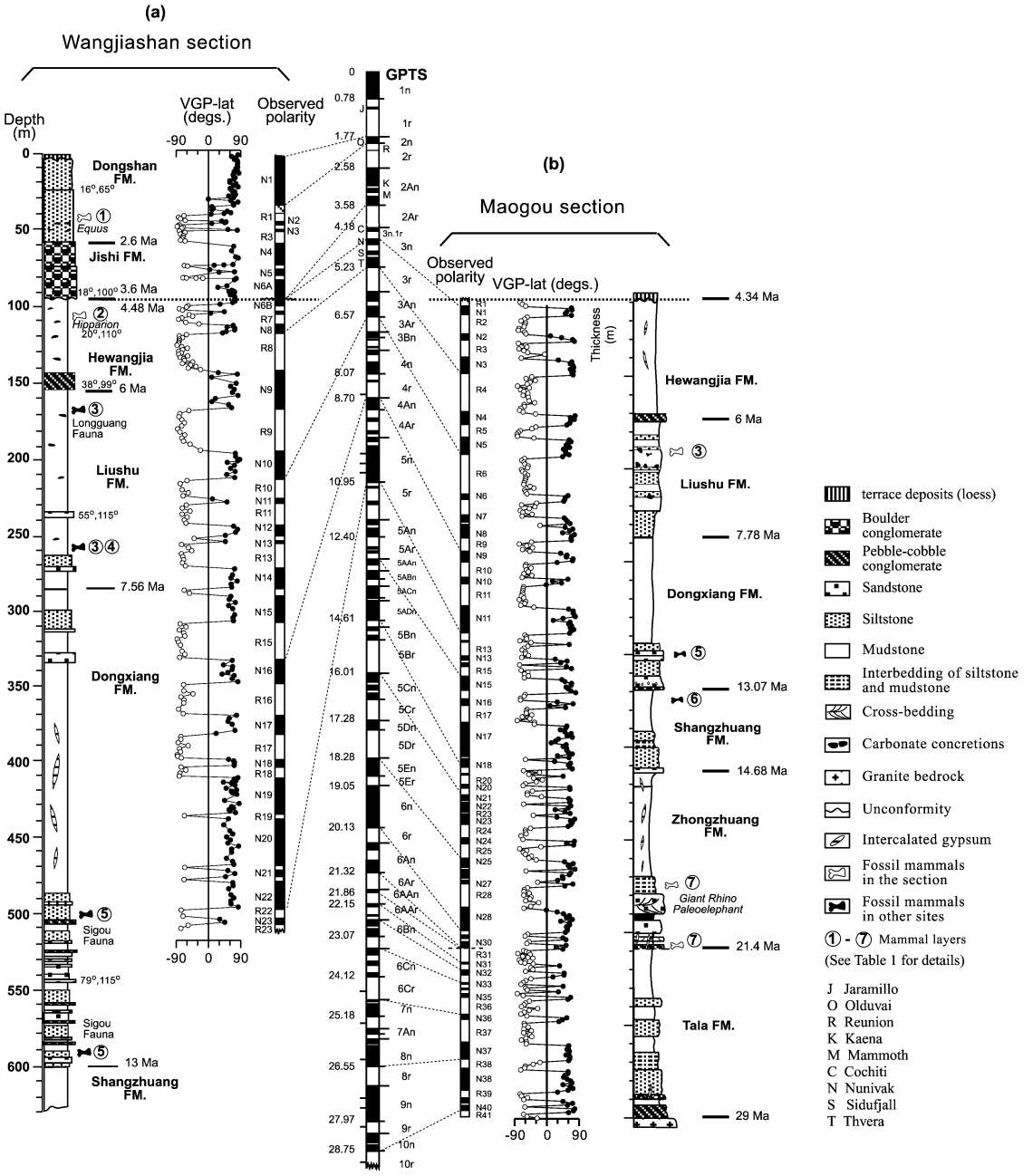

Fig. 3. Correlation of the magnetostratigraphy of the Wangjiashan (a) and Maogou (b) sections with the GPTS of Cande and Kent [24]. Stratigraphic occurrences of fossil mammals found in and near the sections are indicated by circled numbers (detailed in Table 1) and their localities are shown in Fig. 1. For the dipping strata of the Wangjiashan section in panel a, dips and dip directions (dip, direction) are indicated. Major stratigraphic boundary ages calculated from the interpreted sections are shown.

cies. The upper Liushu and Hewangjia formations contain alternating fluvial and lacustrine deposits. Dominantly boulder conglomerate of the Jishi Formation unconformably overlies folded strata in the proximal part of the basin. Grayish-green mudstone, interpreted as deposits of subaqueous loess, of the Dongshan Formation caps the WJS section. Younger loess deposits form a set of terraces along the Yellow River and Daxia River [23].

4. Sampling and analytical methods

Two sections, one at Maogou in the central part of the basin and the other at WJS in the southwestern part of the basin nearer to the Tibetan Plateau (Figs. 1B and 3), were chosen for paleomagnetic study. Fossil mammals were collected from seven localities in the basin, of which four layers lie directly in the studied sections and the other three are very close to the studied sections (Figs. 1B and 3, Table 1). They suggest ages from the Early Miocene to the Early Quaternary (Table 1) [25–32]. Samples were taken at 0.5–1 m stratigraphic intervals in the Maogou section and in the upper 57 m of the WJS section, and at 2 m intervals in the lower 451 m of the WJS section, along 1 m deep trenches through the entire length of the sections. Exceptions were made for the conglomerates where sampling intervals depended on the availability of finer-grained lenses. At each site, one large oriented block was collected from which five or three cubic sub-samples of $2\times2\times2$ cm^3 were taken for the Maogou or WJS sections, respectively. At a later date, additional sub-samples were taken from those levels (sites) where confirmation of the reversal stratigraphy seemed important. A total of 3087 sub-samples (2172 and 915 for the Maogou and WJS sections, respectively) were measured in the laboratories.

The natural remanent magnetization of one set of sub-samples was measured with a Digico magnetometer at Lanzhou University, combined with stepwise alternating-field (AF) demagnetization in 12 steps of 5 mT each up to peak fields of 60 mT. Progressive thermal demagnetization in 15 steps (varying between 10 and 50°C) up to 680°C was carried out for the remaining sub-samples as well as for the supplemental samples collected subsequently. The magnetization behavior during thermal demagnetization was measured with a Schonstedt SSM2 magnetometer at the Chengdu Institute of Geology (for two sets of sub-samples of the Maogou section and for the upper 150 m of the WJS section) and with a 2G cryogenic magnetometer in a magnetically shielded room at the University of Michigan (for the remaining two sets of sub-samples of the Maogou section and for the lower 360 m of the WJS section, and all the supplemental samples).

5. Results

5.1. Paleomagnetic analysis

Representative thermal demagnetization diagrams using the 2G magnetometer show that there are one or two lower blocking temperature components superimposed as overprints on the higher-temperature (characteristic) magnetizations (Fig. 4). The overprints generally have random directions for the lowest blocking temperature intervals (e.g. Fig. 4a–c, <200°C), whereas overprints persisting up to 400°C conform to the present-day geomagnetic field direction. Above 450°C, however, all overprints appear to have been removed and characteristic magnetizations appear to be isolated with clear normal or reversed directions (Fig. 4). Most samples show an accelerated decay in remanent intensity just below 580°C (Fig. 4c,d) or 670°C (Fig. 4a,b), indicating that magnetite and hematite are the major magnetic carriers in these red beds. This is confirmed by the wasp-waisted pattern of the hysteresis measurements of some representative samples of the Maogou section, which are interpreted as showing lower and higher coercivity components coexisting in the samples (Fig. 5a). The high-coercivity component is not saturated at 1.5 T, indicating it is carried by hematite. Curie temperature measurements confirm the high blocking temperatures of hematite above 650°C (Fig. 5b).

About 10% of the directions (mostly from coarse-grained samples) were discarded, mostly

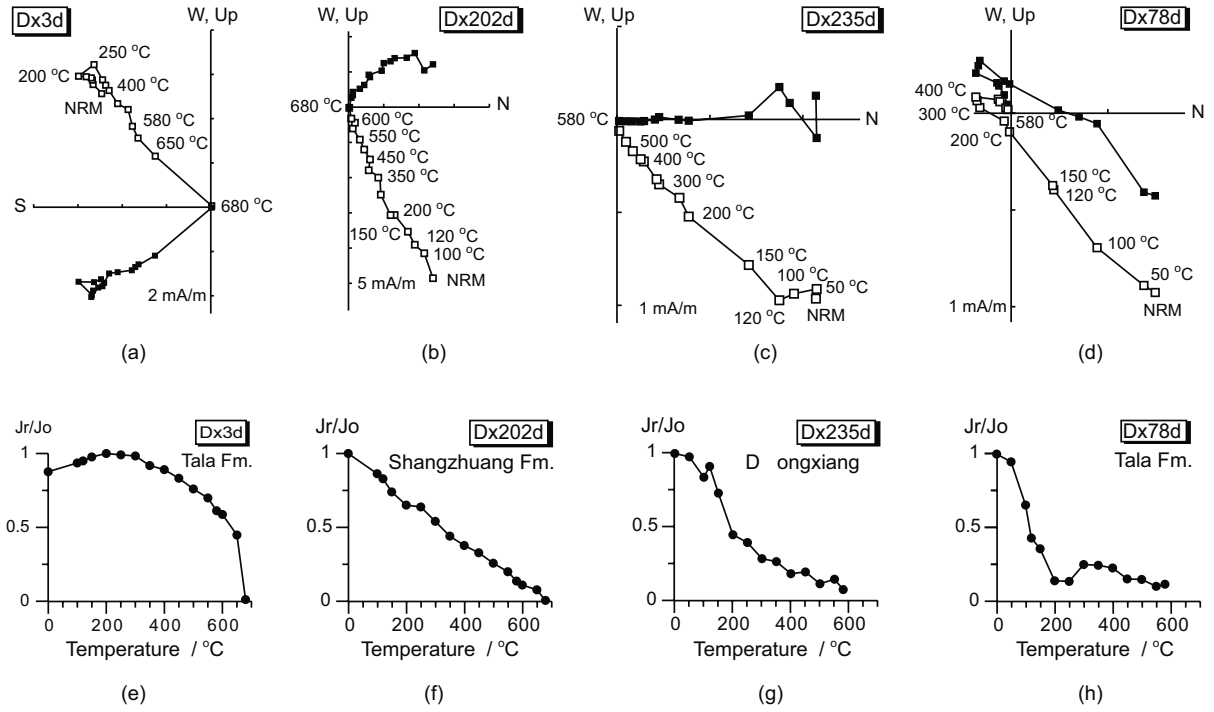

Fig. 4. Thermal demagnetization diagrams of four representative samples with the sample number corresponding to the stratigraphic height in the Maogou section. Full (open) symbols represent projections onto the horizontal (vertical) plane.

because their characteristic remanent magnetization (ChRM) directions could not be determined due to ambiguous or noisy orthogonal demagnetization diagrams, e.g. when maximum angular deviation angles exceeded 15°. Specimens that revealed magnetizations with Virtual Geomagnetic Pole (VGP)-latitude values less than 30° have also been discarded for the calculation of formation-mean directions, but they have been included in the VGP-latitude plots.

Paleomagnetic directions were determined using principal-component analysis of the demagnetization patterns in each sample. The directions obtained in AF demagnetization are generally similar to those of the thermal demagnetizations, but differ to some extent for the purple-red mudstones, where isolation of components is better in thermal demagnetization. Where AF demagnetization of the hematitic beds suggested imperfectly cleaned directions, only the directions obtained in thermal demagnetization were used to calculate site-mean directions. For most thermally demagnetized samples, directions obtained with the Schonstedt SSM2 magnetometer are similar to those from the 2G cryogenic magnetometer, but the latter show more stable behavior for coarse-grained and weak-remanence samples. Mean directions for most sites were obtained by averaging the three or five sub-sample directions at each level. The strata are generally horizontal for the Maogou section, so no structural correction needed to be applied. For the WJS section, tilt corrections were made as described in the original paper [33].

Site-mean directions were used to calculate VGP positions, and the latitudes of these VGPs were used to plot a reversal stratigraphy (Fig. 3) without correcting for the deviation of the formation-mean directions from the present-day field direction. Because the older formations show a mean declination of 14°, interpreted as being caused by local rotations, this introduces a minor

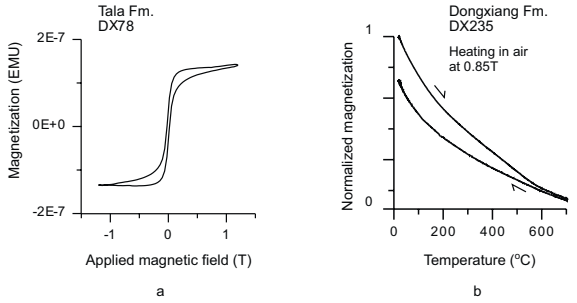

Fig. 5. Hysteresis (a) and Curie temperature (b) measurements of representative samples in the Maogou section. Note the wasp-waisted hysteresis loop, which indicates the co-existence of two (soft and hard) magnetic minerals (panel a). High-coercivity hematite is confirmed by the decay of the magnetization by ~680°C (panel b).

bias in the VGP latitudes. Mean directions for normal, reversed, and combined polarities are listed in Table 2 for each formation.

Fig. 6a shows an equal-area projection of all 418 accepted ChRM directions of the Maogou section. A statistical bootstrap technique [34] has been used to test whether the distributions of the ChRM vectors are possibly non-Fisherian, and to characterize the associated uncertainties for both normal and reversed ChRM directions (Fig. 6b). The histograms of the Cartesian coordinates of bootstrapped means [34] allow us to determine a 95% level of confidence (ovals around the means in Fig. 6a) and to demonstrate that the bootstrap reversal test is positive (Fig. 6b). Furthermore, a jackknife technique [35] was used to quantify the reliability of the magnetostratigraphy. The obtained jackknife parameter (J) for the accepted sample-mean directions has a value of −0.1, which falls within the range of 0 to −0.5 recommended by Tauxe and Gallet [35] for a robust magnetostratigraphic data set, indicating that sampling of the section has recovered more than 95% of the true number of polarity intervals (Fig. 7).

5.2. Summary of the magnetostratigraphic correlations of the WJS section

In order to have an overview of the available Cenozoic magnetostratigraphy of the Linxia Basin and to correlate the WJS magnetostratigraphy with that of the Maogou section, we briefly summarize the previously published [33] magnetostratigraphic results of the WJS section. The studied

Table 2
Paleomagnetic data from the Maogou section, Linxia Basin

	Fm	n/N	Dec	Inc	α_{95}	k	Lat	Lon
Normal polarities	HWJ	23/24	3.2	42.5	7.6	17	78.8	268
	LS	21/21	5.3	38.8	10.4	10.0	75.6	262.8
	DX	40/43	8.3	46.2	6.8	12.0	79.4	239.1
	SZ	27/27	19.7	35.5	13.4	5	73.0	245.2
	ZZ	47/51	9.3	39.7	6.6	11.0	74.7	248.5
	TL	37/38	14.8	39.0	7.5	11.0	71.4	235.2
Reversal polarities	HWJ	44/45	183.5	−38.6	7.8	9.0	75.9	269.5
	LS	30/32	192.8	−31.4	7.6	13.0	68.3	248.1
	DX	44/44	198.1	−39.9	6.0	14.0	69.7	227.3
	SZ	14/14	183.8	−29.2	14.8	8.0	69.8	272.3
	ZZ	37/44	201.4	−38.8	7.7	10.0	66.9	223.3
	TL	54/58	194	−35.9	6.1	11.0	70.1	241.0
Combined	HWJ	67/69	3.4	40	5.7	10	76.9	269
	LS	51/53	9.9	34.5	6.1	12	71.3	253
	DX	84/87	13.7	43	4.6	13	74.2	231
	SZ	41/41	13.7	33.4	10.1	6	72.2	257
	ZZ	84/95	14.6	39.5	5	10	71.7	235
	TL	91/96	14.3	37.2	4.7	11	70.7	239

Fm, Formation; n, number of sites used in calculating a (normal, reversed, or combined-polarity) mean direction; N, total number of sites collected from a formation; Dec, declination; Inc, inclination; k and α_{95}, statistical parameters associated with the means; Lat, latitude; Lon, longitude; HWJ, Hewangjia Formation; LS, Liushu Formation; DX, Dongxiang Formation; SZ, Shangzhuang Formation; ZZ, Zhongzhuang Formation; TL, Tala Formation.

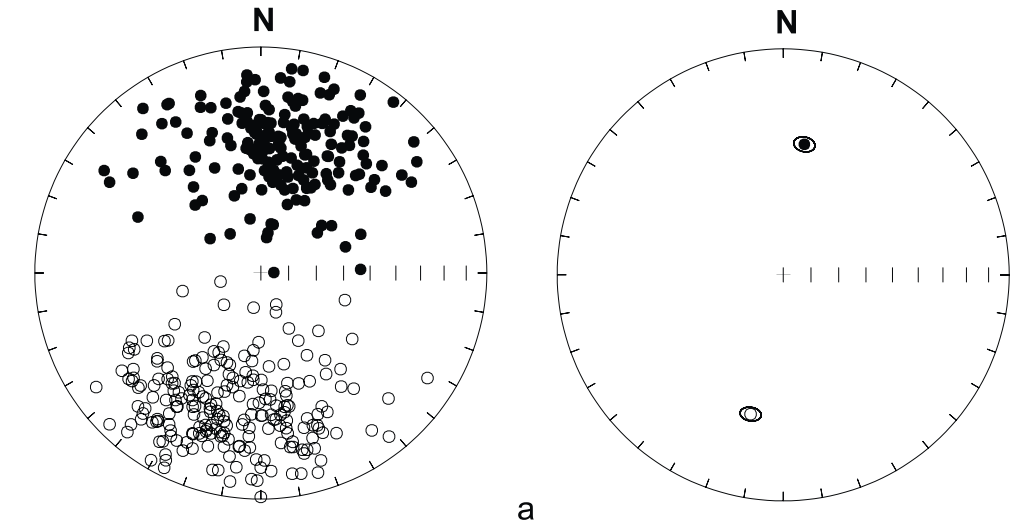

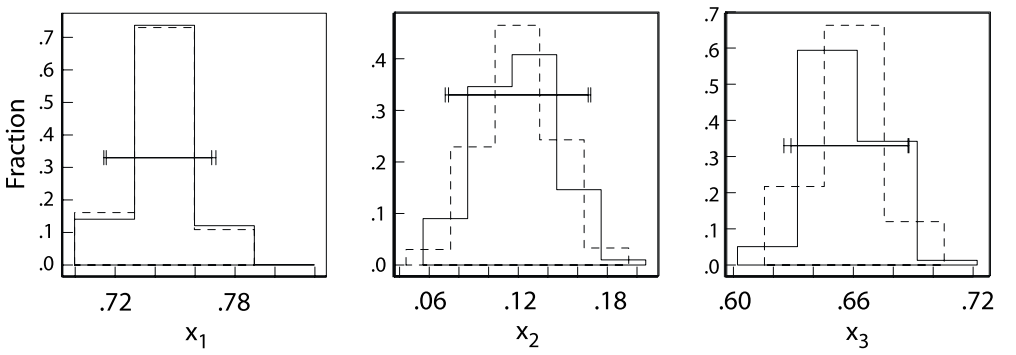

Polarities	Dec	Inc	α_{95}	N	k	Fisherian?
Normal	9.2	41.1	3.2	191	11	No
Reverse	193.2	-36.8	3.1	223	10	No

b

Fig. 6. (a) Equal-area projections of all accepted ChRM directions and the normal- and reversed-polarity mean directions (with ovals of 95% confidence) determined with the bootstrap method [34]. Downward (upward) directions are shown as solid (open) symbols. (b) Bootstrap reversal test diagram. Reversed polarity directions have been inverted to their antipodes to test for a common mean shared by the normal and reversed magnetization directions. The confidence intervals for all components overlap, indicating a positive reversal test.

WJS section (Figs. 1B and 3, left column) shows clean directions recording 23 normal (N1–N23) and 23 reversed zones (R1–R23).

An unconformity at a depth of 94 m splits the magnetostratigraphy into two parts. The uppermost chrons, N1–N3 and R1–R3 in the lacustrine sediments of the Dongshan Formation, are interpreted as representing the Olduvai and Reunion subchrons as well as the lower part of the Matuyama Reversed Chron for two reasons. (1) These intervals can be well correlated both in lithology and magnetostratigraphy to the lower part of yet another section (named Dongshanding, just 5 km south of the WJS section; DS in

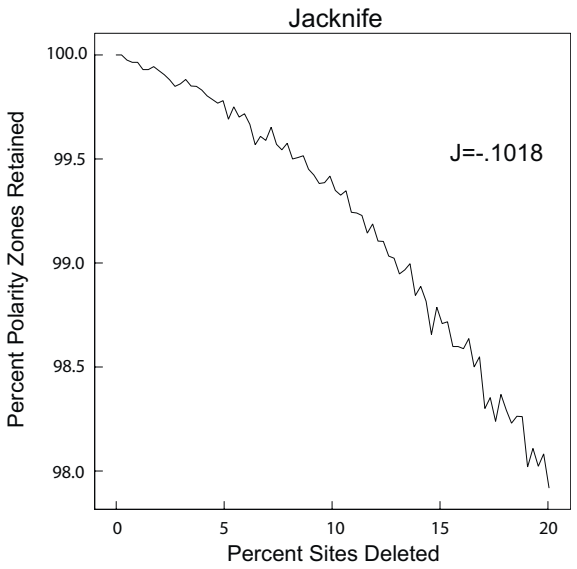

Fig. 7. Magnetostratigraphic jackknife analysis [35] for the Maogou section. The plot indicates the relationship between average percentage of polarity zones retained and the percentage of sampling sites deleted, where the slope J is directly related to the robustness of the results. The slope (J) has a value of -0.1018, which suggests that the section's record has uncovered more than 95% of the true number of polarity intervals.

Fig. 1B), which is complete between the present (Brunhes Chron) and the lower part of the Matuyama Reversed Chron (C2r) [23]. (2) An *equus* and Longdan fauna of Plio–Pleistocene age was found in the lower part of the Dongshan Formation [25] (Table 1 and Fig. 3a). It follows that the intervals N4–N6A below R3 are records of the Gauss Normal Chron (Fig. 3a).

Below the unconformity, the Pliocene fossil mammal *Hipparion* sp. was found in the WJS section in the upper part of the Hewangjia Formation (Fig. 3a). The Longguang and Sigou faunas that were found in the upper part of the Liushu Formation and lower part of the Dongxiang Formation (Figs. 2 and 3) roughly correlate with the Turolian (5.2–9 Ma) [32] and Vallesian (9–12.5 Ma) stages of European land mammals [36] (Table 1), further constraining the age of the immediately overlying Hewangjia Formation. Thus, R6–R7 in the Hewangjia Formation should be part of the Gilbert chrons, with N6B, N7 and N8 correlated, respectively, with the Nunivak, Sidufjall and Thvera subchrons, indicating that the unconformity has eliminated the Cochiti normal event and the uppermost part of the Gilbert [33] (Fig. 3a). Further down, N9 and N10 are correlated with subchrons 3An.1n and 3An.2n. The N19–N22 intervals are the records of the long normal Chron 5n, with other intervals in between correlated with the intervening chrons of the Geomagnetic Polarity Time Scale (GPTS) [24], such as the tie between N16 and Chron 4An, etc.

5.3. *New magnetostratigraphy of the Maogou section and correlations to the GPTS*

Forty normal (N1–N40) and 41 reversed zones (R1–R41) are clearly observed in the Maogou section (Fig. 3b). The N1–N12 intervals in the Hewangjia and Dongxiang formations are easily correlated both in lithologies and magnetozones with those in the WJS section, and equally well with most chrons of the GPTS between chrons 3n and 5n [24]; see, for example, N1–N3, N4–N5 and N11 in the Maogou section and their correlation with chrons 3n.2n–3n.4n, 3An and 5n of the GPTS [24], respectively (Fig. 3). This correlation is also confirmed by Early Pliocene–Late Miocene fossil mammals found in this part of the stratigraphy (Table 1 and Fig. 3b at 360 m). Much lower in the section, at about 100 m, the excavation of very important fossil mammals of paleo-elephant *Gomphotherium* sp. and giant rhinoceros *Rhinocerotidae* gen. indet. as well as other mammals in the lowermost part of the Zhongzhuang Formation both by the authors and other colleagues [28,30] constrain a narrow age of ~21 Ma (early Orleanian of European land mammals or early Burdigalian [28]) (Table 1 and Fig. 3b). An abundance of other mammals of the so-called Shangzhuang fauna were found in the upper part of the Shangzhuang Formation, suggesting an age roughly equivalent to the Astaracian (12.5–15.4 Ma) (Table 1 and Fig. 3b).

Constrained by these three mammal levels (3, 6, and 7 in Fig. 3b), the magnetostratigraphic correlations of N11–N30 are accomplished with most of chrons between 5n and 6An of the GPTS [24]. An example is our correlation of the distinctive long normal zones of N17–N18, N21–N23, and

N28 with chrons 5Acn–5ADn, 5Cn and 6n, respectively (Fig. 3b). In the Tala Formation, below N30, fossil mammals have not yet been found, but observed magnetozones are clean and easily correlated with most chrons between 6AAn.1r and 10r of the GPTS [24] in the Late Oligocene (Fig. 3b). The correlation indicates progressively upward-decreasing sedimentation rates, which agree with fining-upward trends in the sedimentary rocks. It also reveals a hiatus representing chrons 6Ar and 6AAn.1n of the GPTS (Fig. 3b). Thus, an equivalent of ~0.54 Myr is missing in the stratigraphy, indicating the existence of an unconformity between the Tala and Zhongzhuang formations. Granted this correlation, the bottom of the Maogou section is estimated as ~29 Ma. The sedimentary rocks at the bottom of the Maogou section overlie a granite of inferred Paleozoic age, indicating that no deposition took place before the Late Oligocene, and hence, no subsidence has been recorded before 29 Ma.

An age vs. depth plot of the Maogou and WJS sections presents gradually increasing to roughly linear sedimentation rates for the Maogou and WJS sections, respectively, except for some short intervals where rapid sedimentation rates occur, caused by the increased influx of sandstone and/or conglomerate (Fig. 8). This indicates that our interpretation of the magnetostratigraphy of the Maogou and WJS sections is plausible.

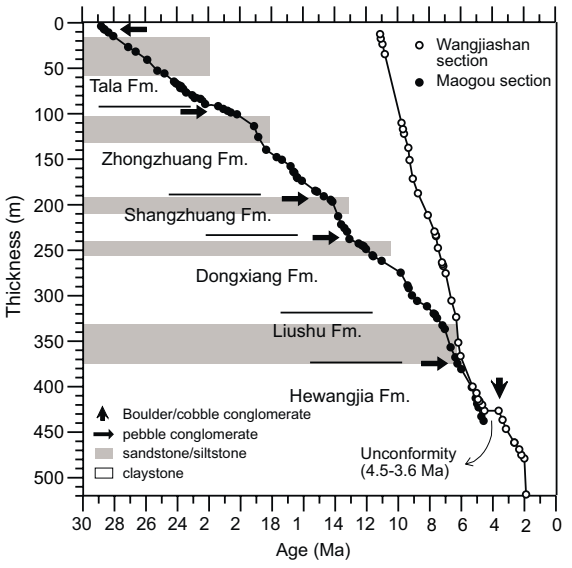

Fig. 8. Age versus thickness relationship of the Wangjiashan [33] and Maogou sections in the Linxia Basin. Data points are taken from the interpreted polarity chrons. Formation names and lithologies are for the Maogou section. Note the higher sedimentary rates that occur in coarser-grained deposits.

5.4. *Rotations deduced from the paleomagnetic directions*

Average declinations of the Maogou section by formation (Table 2 and Fig. 9) demonstrate that the declinations decrease from the older, rather stable, levels (~29–8 Ma) of ~14°, to 9.9° in the Liushu Formation (~8–6 Ma), and then to 3.4° in the Hewangjia Formation (~6–4 Ma). This indicates that the Linxia Basin experienced a clockwise rotation after ~8 Ma, suggesting that contraction of the Linxia Basin by the NE Tibetan Plateau occurred at this time, most probably through the Laijishan thrust (Fig. 1B). The tilting and folding of the strata in the Yingchuangou anticline [33], where the WJS section is located, and a decrease in the sedimentation rate in the Linxia Basin, both beginning at ~6 Ma (Fig. 10), further support the idea of a Late Miocene age for a phase of contraction in the NE Tibetan Plateau. Early Cretaceous declinations in the area [37,38] also show clockwise-deviating declinations.

The average inclinations for the formations range from 34° to 43° and show no temporal trend. The values are lower than expected from the Geocentric Axial Dipole prediction for the area. Neogene results from Central Asia have often revealed such departures, which can be attributed to inclination shallowing during and just after the sedimentation process, or possibly to non-dipole field contributions [39].

6. Discussion

Variation in the stratigraphic thickness and subsidence history of the Linxia Basin provide insight into the mechanisms of subsidence in this region and the history of deformation of the northeastern margin of the Tibetan Plateau.

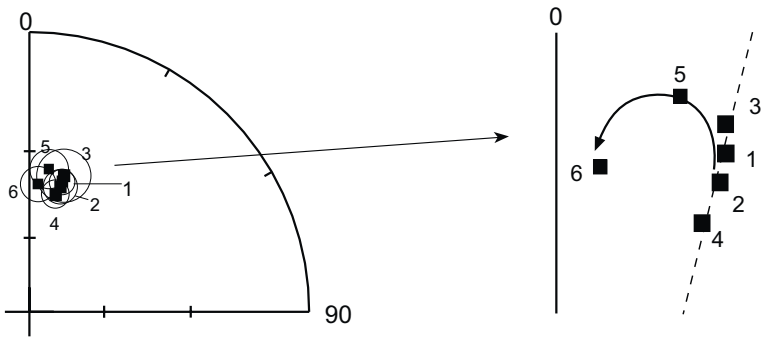

Fig. 9. Equal-area projection of averaged directions (with oval of 95% confidence) for the formations in the Maogou section (see Table 2). 1, Tala Formation; 2, Zhongzhuang Formation; 3, Shangzhuang Formation; 4, Dongxiang Formation; 5, Liushu Formation; 6, Hewangjia Formation. The thin dashed line indicates the mean declination (about +14°) of formations 1–4.

Stratigraphic thickness varies from greater than 1200 m just 20 km northeast of the topographic front of the Tibetan Plateau and thins towards the northeast, pinching out on the southwestern flank of the Maxian Shan (Fig. 1B). The upper 600 m of the thickest section at WJS has been dated by magnetostratigraphy (Figs. 2 and 3), providing chronostratigraphic correlations to the upper Maogou section. Although the lower part of this section has not been dated, lithostratigraphic correlation to the dated Maogou section can be made based on fining-upward cycles documented in both of the sections (Fig. 2). The basement–sediment contact is below the level of incision of the WJS section and therefore cannot be observed. This precludes the determination of an absolute age for initial subsidence in the Linxia Basin. However, based on the lithostratigraphic correlation between the WJS and Maogou sections and an age of 29 Ma for initial sedimentation in the Maogou section, we can infer that subsidence began by 29 Ma at the latest.

Lacustrine, deltaic, and fluvial mudstone and sandstone dominate the basin fill, with greater abundance of fluvial sandstone and conglomerate proximal to the plateau (Fig. 2). Based on variations in stratigraphic thickness, facies patterns, and subsidence rates (Figs. 2 and 10), we suggest that deposition took place in a flexural basin setting, where most of the sediment was sourced from the southwest from the plateau margin. Flexural basins associated with forward-propagating fold-thrust belts display increasing rates of subsidence through time within the foredeep portion of the basin [41]. Forward imbrication in the fold-thrust belt eventually leads to the incorporation of foredeep sedimentary rocks into the fold-thrust belt. In the wedge-top portion of the foreland basin system, synorogenic sediments are deposited in association with active thrust faults at the front of the fold-thrust belt [41]. The wedge-top region is characterized by progressive deformation of strata, lower rates of subsidence, and unconformities [41]. Increasing rates of subsidence from 29 to 6 Ma within the Linxia Basin suggest deposition in the flexural foredeep (Fig. 10). In contrast, a decrease in the rate of subsidence in the proximal part of the basin (at WJS) after

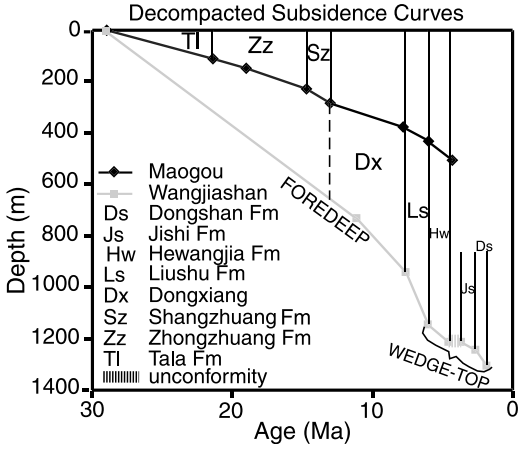

Fig. 10. Subsidence curve for the Wangjiashan and Maogou stratigraphic sections in the Linxia Basin, decompacted by the method of [42].

6 Ma suggests the wedge-top part of the basin had propagated to this location, in agreement with the constraints on the timing of progressive deformation in the WJS section.

The lower WJS section was folded during thrust faulting in the proximal part of the basin, forming the Yingchuangou anticline [33]. Progressive deformation in the WJS section associated with the development of this fold determines the age of thrust faulting in the proximal part of the basin. Bedding dips display rapid shallowing from 38° to 18° beginning at ~6 Ma and continuing until ~3.6 Ma. This thrust faulting may indicate the time at which the Linxia Basin began to be incorporated into the Tibetan Plateau. The thickest succession of boulder conglomerates (Jishi Formation) was deposited in the proximal part of the Linxia Basin beginning ~3.6 Ma and has been interpreted as indicating the age of rapid uplift of the Tibetan Plateau [33,40]. Another possibility is that these deposits reflect the incorporation of the Linxia Basin into the wedge-top part of the foreland basin system, resulting from the forward imbrication of thrust faults on the margin of the Tibetan Plateau. Faulting and folding within the Linxia Basin was followed by rapid intermittent incision of the basin deposits by the Yellow River and Daxia River beginning at ~1.7 Ma. Active thrust faulting and strike-slip faulting north and east of the Linxia sub-basin and Longzhong Basin [2,4,5] indicate that these basins are currently caught up in the deformation of the northeastern margin of the Tibetan Plateau.

The timing of initial deformation of northeastern Tibet has implications for the growth history of the Tibetan Plateau. Initial deformation in the eastern Qiantang Block is documented as Cretaceous–Eocene in age [9,10]. By Late Oligocene time, deformation had propagated into the Songpan–Ganzi and Kunlun–Qaidam terranes, as evidenced by the subsidence history in the Linxia Basin and magnetostratigraphic constraints on the timing of thrusting in the Nan Shan fold-thrust belt [14]. On the eastern margin of the Tibetan Plateau in the Longmen Shan, $^{40}Ar/^{39}Ar$ and (U–Th)/He thermal histories indicate an increase in exhumation in Late Miocene–Early Pliocene time [43]. The onset of rapid cooling in this region is interpreted as marking the onset of deformation that led to the development of the eastern part of the plateau and produced the steep topographic gradient observed today between the Sichuan Basin and the plateau. These interpretations agree with the subsidence history in the Linxia Basin, which shows a decrease in subsidence at ~6 Ma, eventually leading to the uplift and incision of Linxia Basin fill. It is also at about this time that the basin underwent a clockwise rotation of some 10°, as can be deduced from the decreasing declination values of the Liushu and Hewangjia formations (7.5–4.5 Ma). All of these lines of evidence point to the initial incorporation of this region into the Tibetan Plateau beginning by ~7.5–6 Ma.

The relationship between strike-slip deformation and shortening in northeastern Tibet is still unclear. Flexural basins in eastern Qiangtang are cut by younger strike-slip faults [9], suggesting that these Cretaceous–Eocene basins are not related to strike-slip deformation. Along the Altyn Tagh fault, different data sets suggest that strike-slip deformation may have begun as early as 49 Ma [14] or as late as Late Oligocene to earliest Miocene time [15]. An Eocene age for initial motion on the Altyn Tagh fault leaves open the possibility that strike-slip faulting accommodated regional transpression in northeastern Tibet in Oligocene time. Documentation of the timing of earliest motion on large strike-slip faults to the south of the Altyn Tagh fault, such as the Kunlun fault, is critical to understanding the role of strike-slip deformation in crustal shortening in northeastern Tibet.

7. Conclusions

1. New magnetostratigraphic results from the Maogou section allow us to assign ages between 29 and 1.7 Ma to the Cenozoic formations in the Linxia Basin. Previous magnetostratigraphic results from the WJS section correlate well with those for the upper half of the Maogou section.
2. Linxia Basin deposits both thin and fine towards the northeast, away from the topo-

graphic front of the Tibetan Plateau. Subsidence rates in the Linxia Basin increase through time until ~6 Ma in the proximal part of the basin. These observations suggest subsidence by flexural loading during the thickening of the northeastern margin of the Tibetan Plateau between ~29 and 6 Ma.

3. A decrease in subsidence rates at 6 Ma coincides with progressive deformation associated with initial thrusting in the proximal part of the basin and a clockwise rotation of the basin of about 10°. These data indicate that the deformation front of the Tibetan Plateau had propagated into this region by 6 Ma.
4. Initial deformation is documented in the eastern Qiangtang Block in Cretaceous–Eocene time [9,10]. This study demonstrates that deformation began in the Songpan–Ganzi and Kunlun–Qaidam terranes by Late Oligocene time. By ~6 Ma, deformation had propagated towards the east [43] and northeast beyond Linxia. This age progression in deformation suggests that the NE margin of the Tibetan Plateau grew in a stepwise fashion towards the northeast through time.

Acknowledgements

This work was co-supported by the MOE Key Project on Sci-Technology Research, Chinese Academy of Science (Grant No. Ren-Jiao-Zi [2000]005), the Chinese National Key Projects for Basic Research on Tibetan Plateau (Grant No. G1998040809), and the U.S. National Science Foundation (Grant EAR 9903074 to R.V.d.V.). We thank Song Chunhui for assistance in the field, M. Torii and N. Ishikawa for assistance in the laboratory for measuring hysteresis and Curie temperatures of some selected samples, and the journal's reviewers (Neil D. Opdyke, Katherine Giles and anonymous) for their constructive comments.*[SK]*

References

[1] P. Molnar, H. Lyon-Caen, Fault plane solutions of earthquakes and active tectonics of the Tibetan Plateau and its margins, Geophys. J. Int. 99 (1989) 123–153.
[2] P. Tapponnier, B. Meyer, J.P. Avouac, G. Peltzer, Y. Gaudemer, S. Guo, H. Xiang, K. Yin, Z. Chen, S. Cai, H. Dai, Active thrusting and folding in the Qilian Shan and decoupling between upper crust and mantle in northeastern Tibet, Earth Planet. Sci. Lett. 97 (1990) 382–403.
[3] P. Zhang, B.C. Burchfiel, P. Molnar, W. Zhang, D. Jiao, Q. Deng, Y. Wang, L. Royden, F. Song, Amount and style of late Cenozoic deformation in the Liupan Shan area, Ninxia autonomous region, Chin. Tecton. 10 (1991) 1111–1129.
[4] Y. Gaudemer, P. Tapponnier, B. Meyer, G. Peltzer, S. Guo, Z. Chen, H. Dai, I. Cifuentes, Partitioning of crustal slip between linked, active faults in the eastern Qilian Shan, and evidence for a major seismic gap, the 'Tianzhu gap', on the western Haiyuan Fault, Gansu (China), Geophys. J. Int. 120 (1995) 599–645.
[5] B. Meyer, P. Tapponnier, L. Bourjot, F. Métivier, Y. Gaudemer, G. Peltzer, S. Guo, Z. Chen, Crustal thickening in Gansu-Qinghai, lithospheric mantle subduction, and oblique, strike-slip controlled growth of the Tibet Plateau, Geophys. J. Int. 135 (1988) 1–47.
[6] B.C. Burchfiel, Q. Deng, P. Molnar, L. Royden, Y. Wang, P. Zhang, W. Zhang, Intracrustal detachment zones of continental deformation, Geology 17 (1989) 448–452.
[7] Z. Chen, B.C. Burchfiel, Y. Liu, R.W. King, L.H. Royden, W. Tang, E. Wang, J. Zhao, X. Zhang, Global Positioning System measurements from eastern Tibet and their implications for India/Eurasia intercontinental deformation, J. Geophys. Res. 105 (2000) 16215–16227.
[8] P. Tapponnier, Z. Xu, F. Roger, B. Meyer, N. Arnaud, G. Wittlinger, J. Yang, Oblique stepwise rise and growth of the Tibet Plateau, Science 294 (2001) 1671–1677.
[9] B.K. Horton, A. Yin, M.S. Spurlin, J. Zhou, J. Wang, Paleocene-Eocene syncontractional sedimentation in narrow, lacustrine-dominated basins of east-central Tibet, Geol. Soc. Am. Bull. 114 (2002) 771–786.
[10] F. Roger, P. Tapponnier, N. Arnaud, U. Schärer, M. Brunel, Z. Xu, J. Yang, An Eocene magmatic belt across central Tibet: mantle subduction triggered by Indian collision?, Terra Nova 12 (2000) 102–108.
[11] M. Jolivet, M. Brunel, D. Seward, Z. Xu, J. Yang, F. Roger, P. Tapponnier, J. Malavieille, N. Arnaud, C. Wu, Mesozoic and Cenozoic tectonics of the northern edge of the Tibetan Plateau: fission tract constraints, Tectonophysics 343 (2001) 111–134.
[12] E. Sobel, N. Arnaud, M. Jolivet, B.D. Ritts, M. Brunel, Jurassic to Cenozoic exhumation history of the Altyn Tagh range, northwest China, constrained by $^{40}Ar/^{39}Ar$ and apatite fission track thermochronology, in: M.S. Hendrix, G.A. Davis (Eds.), Paleozoic and Mesozoic Tectonic Evolution of Central Asia: From Continental Assembly to Intracontinental Deformation, Geol. Soc. Am. Mem. 194, 2001, pp. 247–267.
[13] A.W. Bally, R.T. Ryder, H.P. Euster, Comments on the geology of the Qaidam basin, in: Notes on Sedimentary Basins in China, Report of the American Sedimentary Basins Delegation to the People's Republic of China, U.S. Geol. Surv. Open-File Rep. 86-327, 1986, pp. 42–62.
[14] A. Yin, P.E. Rumelhart, R. Butler, E. Cowgill, T.M. Har-

rison, D.A. Foster, R.V. Ingersoll, Q. Zang, X.Q. Zhou, X.F. Wang, A. Hanson, A. Raza, Tectonic history of the Altyn Tagh fault system in northern Tibet inferred from Cenozoic sedimentation, Geol. Soc. Am. Bull. 114 (2002) 1257–1295.

[15] Y. Yue, B.D. Ritts, S.A. Graham, Initiation and long-term slip history of the Altyn Tagh fault, Int. Geol. Rev. 43 (2001) 1–7.

[16] A.D. Hanson, Cenozoic basin evolution of southern Tarim, northwestern China: Implications for the uplift history of the Tibetan Plateau, Thesis, Stanford University, 1999.

[17] A.D. George, S.J. Marshallsea, K. Wyrwoll, J. Chen, Y. Lu, Miocene cooling in the northern Qilian Shan, northeastern margin of the Tibetan Plateau, revealed by apatite fission-track and vitrinite-reflectance analysis, Geology 29 (2001) 939–942.

[18] W. Xu, Y. He, Y. Yan, Tectonic characteristics and hydrocarbons of the Hexi Corridor, in: X. Zhu (Ed.), Chinese Sedimentary Basins, Elsevier, Amsterdam, 1989, pp. 52–62.

[19] Gansu Geologic Bureau, Regional Geologic History of Gansu Province, Geologic Publishing House, Beijing, 1989.

[20] A. Yin, S. Nie, An indentation model for North and South China collision and the development of the Tanlu and Honam fault systems, eastern Asia, Tectonics 12 (1993) 801–813.

[21] D. Zhou, S.A. Graham, The Songpan-Ganzi complex of the western Qinling Shan as a Triassic remnant ocean basin, in: A. Yin, T.M. Harrison (Eds.), The Tectonic Evolution of Asia, Cambridge University Press, Cambridge, 1996, pp. 281–299.

[22] O. Bruguier, J.R. Lancelot, J. Malavieille, U-Pb dating on single detrital zircon grains from the Triassic Songpan-Ganzi flysch (Central China): provenance and tectonic correlations, Earth Planet. Sci. Lett. 152 (1997) 217–231.

[23] J. Li, X. Fang, R. Van der Voo, J. Zhu, C. MacNiocaill, Y. Ono, B. Pan, W. Zhong, J. Wang, T. Sasaki, Y. Zhang, J. Cao, S. Kang, J. Wang, Magnetostratigraphic dating of river terraces Rapid and intermittent incision by the Yellow River of the northeastern margin of the Tibetan Plateau during the Quaternary, J. Geophys. Res. 102 (1997) 10121–10132.

[24] S.C. Cande, D.V. Kent, Revised calibration of the geomagnetic polarity timescale for the Late Cretaceous and Cenozoic, J. Geophys. Res. 100 (1995) 6093–6095.

[25] Gansu Regional Geological Survey Team (GRGST), Introduction to the 1:200,000 Geological Map of the People's Republic of China: Linxia - Lanzhou, 1965.

[26] Gansu Regional Geological Survey Team (GRGST), Tertiary System of Gansu - Gansu Geology, 1984.

[27] Z.X. Qiu, J.Y. Xie, D.F. Yan, The new discovery of Chilotherium in Hezheng County of Gansu Province, China, Sci. Sin. 5 (1987) 545–552.

[28] Z.X. Qiu, H.Y. Xie, D.F. Yan, Discovery of some early Miocene mammalian fossils from Dongxiang, Gansu, Vertebr. Palasiatica 28 (1990) P-24.

[29] Z.X. Qiu, B.Y. Wang, T. Deng, X.J. Ni, X.M. Wang, Notes on the mammal fauna from the bottom of loess deposits at Longdan, Dongxiang County, Gansu Province, Quat. Sci. 22 (2002) 33–38.

[30] Z.G. Gu, S.H. Wang, S.Y. Hu, D.T. Wei, Research progress on biostratigraphy of Tertiary Red Beds in Linxia Basin, Gansu Province, in: Study on the Formation and Evolution of the Qinghai-Xizang Plateau, Environmental Change and Ecological System, Science Press, Beijing, 1995, pp. 91–95.

[31] Z.G. Gu, S.H. Wang, S.Y. Hu, D.T. Wei, Discovery of Giraffokeryx in China and the Tertiary chronostratigraphy of Linxia, Gansu Province, Chin. Sci. Bull. 40 (1995) 758–760.

[32] J.Y. Xie, Neogene stratigraphy and fossil mammals of Gansu, J. Stratigr. 15 (1991) 35–41.

[33] J. Li, X. Fang, R. Van der Voo, J. Zhu, C. MacNiocaill, J. Cao, W. Zhong, H. Chen, J. Wang, J. Wang, Y. Zhang, Late Cenozoic magnetostratigraphy (11-0 Ma) of the Dongshanding and Wangjiashan sections in Longzhong Basin, western China, Geol. Mijnb. 76 (1997) 121–134.

[34] L. Tauxe, Paleomagnetic Principles and Practice, Kluwer Academic, Dordrecht, 1998, 299 pp.

[35] L. Tauxe, Y. Gallet, A jackknife for magnetostratigraphy, Geophys. Res. Lett. 18 (1991) 1783–1786.

[36] W.A. Berggren, J.A. Van Couvering, The late Neogene: biostratigraphy, geochronology, and paleoclimatology of the last 15 million years in marine and continental sequences, Palaeogeogr. Palaeoclimatol. Palaeoecol. 16 (1974) 1–216.

[37] N. Halim, J.P. Cogné, Y. Chen, R. Atasiesi, J. Besse, V. Courtillot, S. Gilder, J. Marcoux, R.L. Zhao, New Cretaceous and early Tertiary paleomagnetic results from Xining-Lanzhou basin, Kunlun and Qiangtang blocks, China: Implications on the geodynamic evolution of Asia, J. Geophys. Res. 103 (1998) 21025–21045.

[38] T. Yang, Z. Yang, Z. Sun, A. Lin, New Early Cretaceous paleomagnetic results from Qilian orogenic belt and its tectonic implications, Sci. China D 45 (2002) 565–576.

[39] J. Si, R. Van der Voo, Too-low magnetic inclinations in Central Asia: An indication of a long-term Tertiary non-dipole field?, Terra Nova 13 (2001) 471–478.

[40] J. Li et al., Uplift of Qinghai - Xizang (Tibet) Plateau and Global Change, Lanzhou University Press, Lanzhou, 1995, 207 pp.

[41] P.G. DeCelles, K.A. Giles, Foreland basin systems, Basin Res. 8 (1996) 105–123.

[42] J.G. Sclater, P.A.F. Christie, Continental stretching: An explanation of the post Mid-Cretaceous subsidence of the central North Sea Basin, J. Geophys. Res. 85 (1980) 3711–3739.

[43] E. Kirby, K.X. Whipple, B.C. Burchfiel, W. Tang, G. Berger, Z. Sun, Z. Chen, Neotectonics of the Min Shan, China: Implications for mechanisms driving Quaternary deformation along the eastern margin of the Tibetan Plateau, Geol. Soc. Am. Bull. 112 (2000) 375–393.